Sexual Dimorphism in c-Fos Networks Governing Aggression

Antonio Aubry[1,2,*], Long Li[3,4,#], Romain Durand-de Cuttoli[1,2,#], Elizabeth Karpman[5], Hyoseon Oh[1,2], Arman A. Tavallaei[1,2], Scott Russo[1,2,*]

[1] Nash Family Department of Neuroscience, Icahn School of Medicine at Mount Sinai, New York, New York, USA
[2] Brain & Body Research Center and Friedman Brain Institute, Icahn School of Medicine at Mount Sinai, New York, New York, USA
[3] State Key Laboratory of Brain and Cognitive Science, Institute of Biophysics, Chinese Academy of Sciences, Beijing 100101, China.
[4] University of the Chinese Academy of Sciences, Beijing 100049, China.
[5] Department of Pharmacology, UT Health San Antonio Long School of Medicine
[6] Mayo Clinic Graduate School of Biomedical Sciences
[#] Equal Contribtuion
* Co-corresponding: Antonio.Aubry@mssm.edu, scott.russo@mssm.edu

Abstract

Circuit based studies of aggression often focus on the output of a small group of regions referred to as the "core aggression circuit," yet a whole-brain map of activity has yet to be produced. Using resident–intruder assays in male and female Swiss Webster mice, we combined iDISCO+ c-Fos imaging with a weighted co-expression network analyses to identify mesoscale co-activation modules in aggressive (AGG) vs. non-aggressive (NON) animals. We performed a module preservation analysis between each phenotype within each sex followed by differential correlation to localize edge-level changes. Behaviorally, AGG mice spent more time attacking, while females showed greater social investigation. Network analyses revealed that NON networks often preserved density of AGG modules, but connectivity reorganized with aggression. In male AGGs there was large spread reorganization of numerous modules: a large sensorimotor–subcortical "blue" module, a pallidal/hypothalamic/brainstem "yellow" module, and a brainstem-heavy "green" module. Surprisingly the "brown" module, enriched for classic social-behavior regions was moderately preserved in male NONs. In females, the turquoise module spanning somatosensory/interoceptive cortex and midbrain regions and the "brown" sensory cortex-amygdala module were the least preserved. These results indicate that aggression recruits distributed mesoscale communities via edge-specific gain, with males displaying broad strengthening along a cortex/basal ganglia/ hypothalamus/brainstem axis and females showing more targeted potentiation within sensory/arousal modules. This framework nominates candidate hubs and edges for causal manipulation.

Introduction

Aggression is an evolutionarily conserved behavior that controls social hierarchies and protects valuable resources (Lischinsky & Lin, 2020; Wei et al., 2021). In the wild, aggression is a necessary, adaptive component of social behavior. In humans, however, some forms of

aggression are considered pathological when they threaten lives, increase the risk of psychiatric impairment in victims pointing to the need for identifying targets for therapeutic interventions (Golden, Jin, Heins, et al., 2019; Golden, Jin, & Shaham, 2019; Kessler et al., 2006; McCloskey et al., 2010). Research on aggression has focused on a few brain regions termed the "core aggression circuit" (CAC) in mostly male mice (Mei et al., 2023). The CAC largely overlaps with the "social behavior network" which was largely identified by examining c-fos in a handful of regions that expression steroid hormone receptors (Goodson, 2005; Lawal et al., 2025; Newman, 1999) such as medial amygdala (Hong et al., 2014; Unger et al., 2015), the ventrolateral portion of the ventromedial hypothalamus (Falkner et al., 2016; Hashikawa et al., 2017; Lee et al., 2014; Lin et al., 2011; Mountoufaris et al., 2024; Yan et al., 2024), the posterior portion of the bed nucleus of the stria terminalis(Bayless et al., 2019; Yang et al., 2022), and the ventral pre-mammillary nucleus(Chen et al., 2020; Stagkourakis et al., 2018). Recent work also indicates that regions of the pallial amygdala such as the posterior amygdala (Yamaguchi et al., 2020; Zha et al., 2020) and the posterolateral cortical amygdala (Aubry et al., 2025) are also part of this network.

While studying these regions has led to great progress in understanding the neural circuits of aggression, the mouse brain contains hundreds of regions, which leaves open the possibility that the network of regions which play a significant role in aggression is larger than expected(Simpson et al., 2021). Unbiased, whole-brain approaches are therefore needed to reveal how large-scale functional networks reorganize depending on which behaviors the animal engages in. Indeed, recent c-Fos mapping combined with network analyses has demonstrated how interregional coactivation patterns are altered as a result of fear memory consolidation (Roy et al., 2022; Vetere et al., 2017) and exposure to alcohol (Ardinger et al., 2024; Kimbrough et al., 2020; Roland et al., 2023), complementing region-focused analyses and reducing a priori bias toward canonical circuits.

In this paper, we used whole-brain c-fos mapping combined with a behavioral paradigm which elicits aggression in both male and female outbred Swiss Webster mice (Aubry et al., 2022; Newman et al., 2019). We then adopted the Weighted Gene Co-expression Network Analysis (WGCNA) framework (Langfelder & Horvath, 2008; Zhang & Horvath, 2005) to our c-fos data to identify mesoscale modules of co-activation in aggressive (AGG) and non-aggressive (NON) males and females. We then quantified module preservation between AGGs and NONs within each sex using permutation-based preservation statistics of module density and connectivity to test which modules are reorganized in AGGs relative to NONs (Langfelder et al., 2011). Finally, within modules that show altered organization, we perform differential correlation to localize the specific region pairs whose adjacencies differ significantly between AGG and NON (McKenzie et al., 2016).

Results

Social Behavior in male and females

We quantified various social behaviors on the day mice were euthanized for whole brain quantification of c-fos expression (Fig. 1A) As expected we found that both AGG male and female mice engaged in aggressive behavior for a longer period of time than NONs ($F_{(1,69)} = 54.14$, $p < 0.0001$, Fig 1B). When examining gross interaction, we found that females ($F_{(1,69)} = 27.62$, $p <$

0.001) engaged in more investigation than males of each phenotype (NONs: $p < 0.001$, AGGs: $p = 0.0315$, Fig. 1C). We next examined investigation of distinct body parts and found that females investigated the intruders anogenital region ($F_{(1,69)} = 14.87$, $p = 0.0003$), face ($F_{(1,69)} = 33.63$, $p < 0.0001$) and flank ($F_{(1,69)} = 7.330$, $p = 0.0085$) more than males. We also found a Phenotype x Sex significant interaction for facial investigation ($F_{(1,69)} = 6.591$, $p = 0.014$) and flank investigation ($F_{(1,69)} = 5.346$, $p = 0.0238$). Post-hoc comparisons revealed that female AGGs engaged in more facial investigation than female NONs ($p = 0.0459$) and male AGGs ($p < 0.0001$). In contrast, female NONs engaged in more flank investigation than female AGGs ($p = 0.0058$) and male NONs ($p = 0.0019$). When examining distinct attack behaviors, we did not find a difference between biting ($t_{(33.91)} = 0.04829$, $p = 0.9618$) or kicking ($t_{(29.46)} = 1.829$, $p = 0.0776$), but males engaged in more wrestling behavior than females ($t_{(21)} = 2.316$, $p = 0.0307$).

Region of interest based analysis

Across the 278 regions sampled, the aggressive phenotype produced a coherent elevation of c-Fos from neocortex to medulla, whereas sex differences were more spatially restricted. In the Isocortex, hippocampus and amygdala, (Fig 2A), AGGs showed increased activity in primary and secondary motor cortex (primary motor area, MOp; secondary motor area, MOs), granular and agranular insular cortex (AI), and temporal association cortex (TEA), as well as in olfactory recipient amygdalar areas and the piriform cortex. The entire amygdala complex—including the lateral (LA), basolateral (BLA), basomedial (BMA), central (CEA), medial (MEA) and cortical (COAp) nuclei—was similarly up-regulated in AGGs. When comparing between the sexes, females showed higher c-Fos in motor and medial frontal cortices (infralimbic/prelimbic, anterior cingulate dorsal and ventral, orbital lateral/ventrolateral), whereas males exhibited greater activation in higher-order visual fields (posteromedial and anteromedial visual cortex, VISpm/VISam), retrosplenial cortex (RSPd/RSPv/RSPagl), the hippocampal formation (cornu ammonis 1 and 3, CA1/CA3, and dentate gyrus, DG), and select pallial amygdala nuclei (BMA, BLAv).

Within the basal ganglia, thalamus, and hypothalamus (Fig. 2B), AGGs engaged numerous regions of the ventral striatum including the nucleus accumbens (ACB), fundus striati (FS), and olfactory tubercle (OT), as well as extended pallidal structures (globus pallidus, GP; bed nucleus of the stria terminalis, BST; substantia innominata, SI). Thalamic sensory and associative relays (subparafascicular, SPF; posterior, PO/PP; medial geniculate, MG; lateral posterior, LP; anterodorsal, AD; paracentral, PCN) and canonical hypothalamic aggression loci (dorsomedial hypothalamus, DMH; lateral hypothalamic area, LHA; lateral preoptic area, LPO; posterior hypothalamus, PST; tuberal nucleus, TU) were likewise activated. Sex differences were muted in this sector: males showed higher c-Fos counts than females in a subset of sensory thalamic relays (posterior, medial geniculate, anteromedial, AM) and in paraventricular (PVp), medial mammillary (MM), and ventromedial (VMH) hypothalamic nuclei.

In the midbrain and pons (Fig. 2C), aggression recruited multiple layers of the superior colliculus (superficial, intermediate, deep), the periaqueductal gray (PAG), ventral tegmental area (VTA), and serotonergic dorsal raphe (DR). Pontine arousal centers such as the locus coeruleus (LC), laterodorsal (LDT) and sublaterodorsal (SLD) tegmental nuclei, rostral pontine reticular nucleus (RPO), and nucleus incertus (NI) were likewise activated. Sex comparisons revealed that males-

showed increased countd in the midbrain reticular nucleus (MRN), VTA, and the optic layer of the superior colliculus (SCop).

There were modest phenotypic differences in the medulla and cerebellum (Fig. 2D). AGGs displayed heightened c-Fos in the vestibular nuclei of the medulla and cerebellar nuclei such as the Interposed (IP) and Fastigial (FN) nuclei. Relative to females, males showed selectively higher activation in rerticular nuclei of the medulla, such as the Magnocellular (MARN) and Parvocellular (PARN) reticular nuclei, and the Paragigantocellular reticular nucleus (PGRN) and in the vermal regions of the cerebellum (Lingula, Central Lobule and Culmen).

Sex-Specific Region of interest based analysis

In the isocortex, hippocamps and amygdala (Fig. 3A), aggression in males triggered a rise in c-Fos in the MOp and the full somatosensory cortex (SSP-bfd/ll/m/n/tr/ul)—as well as gustatory (GU), visceral (VISC), auditory (AUDd/p/v) and higher visual cortices (VISal, VISl, VISp). Activity also spread into the granular and agranular insula (AI) and retrosplenial cortex (RSP). Females, by contrast, showed an increase in frontal cortical regions (MOs, infralimbic (IL), orbital (ORB)) and in higher-order visual fields (VISal, VISl, VISpl). There were also increased activation in anterior olfactory/cortical regions (taenia tecta (TT), dorsal peduncular (DP), and the anterior olfactory nucleus (AON)). In the amygdala complex male AGGs showed increases in every major amygdalar region (LA, BLAa/v/p, BMA,CEA, MEA, and COAp), together with the ventral striatal regions (ACB, FS, OT). Females recruited only a subset of these limbic regions (BLAv, BMA, the anterior amygdala area (AAA) and ACB), marking these as the core limbic areas activated by aggression common to both sexes.

There were large sex-specific differences in AGGs in the basal ganlia, thalamus and hypothalamus. In males, sensory-relay thalamic nuclei (PO, MG, LP) and intralaminar hubs (PCN, CM, CL) showed significant activation, accompanied by canonical hypothalamic aggression loci: dorsomedial (DMH), lateral (LHA), VMH, lateral preoptic (LPO) and posterior hypothalamus (PST). Female AGGs showed increases only in the intralaminar thalamus (PCN, CM, CL) without significant activation in the hypothalamus, suggesting a male-biased hypothalamic drive.

Aggression-linked activation in the midbrain arousal showed common areas of activation in various midbrain regions. Males display tectal–mesencephalic activation in the superficial and deep layers of the superior colliculus (SCop/sg/dg/dw), the inferior colliculus (IC), periaqueductal grey (PAG), substantia nigra pars compacta (SNc), ventral tegmental area (VTA), and the dorsal raphe (DR). Females engage a small number of regions centered on the deep superior colliculus, PAG, cuneiform (CUN), DR and locus coeruleus (LC). These shared regions delineate a conserved midbrain core that likely orchestrates the autonomic facets of aggression.

The hindbrain and cerebellum also revealed sex-specific differences in AGGs. Males show activation in reticulospinal and autonomic centers across the pons and medulla (rostral pontine reticular nucleus (RPO), lateral tegmental nucleus (LTN), gigantocellular nucleus (GRN)), and in the cerebellar fastigial (FN), culmen (CUL), and simple lobule (SIM). Females, in contrast, only showed significant activation of the inferior olive (IO) and the cerebellar vermis lobule (VERM).

Together, these observations show that the aggressive state mobilizes a brain-wide high-gain mode in males that sweeps from primary sensory cortex to medullary effectors, whereas females activate a slimmer, strategically placed network anchored in association cortex, nucleus accumbens, select amygdaloid nuclei, thalamic intralaminar hubs and the core midbrain arousal system.

Whole Brain Network Analyses

To understand how these regions are co-activated in male and female AGGs, we applied the weighted-gene co-expression network analysis (WGCNA) framework to our data set. We constructed a network for each of the four groups and then preformed a module preservation analysis for each sex with the AGG network set as the reference network. We found that the NON networks for each sex were able to preserve the density of connections in the identified modules (Supplementary Table 1 & 2), however we found that the specific connectivity profiles were not preserved in select modules from male and female AGGs.

In males, the blue module was a large cluster linking together numerous cortical areas with the basal ganglia, septum, thalamic relay areas and superior colliculus sub laminae (Fig 4A). Of the 77 total regions in this cluster, 66 showed significant differences in their total connection strength with other regions in the module. Of these 66, AGG mice showed higher connectivity strengths in 63 of the 66. Given that the connectivity profiles include both direct connections between each pair of regions and their shared connections with all other nodes in the cluster, we performed a differential correlation analysis on the regions which showed significantly different connection strengths to examine pairwise correlations. Of the 2016 correlations evaluated, 309 showed a significant difference between the AGG and NON modules (Fig.4C). Of the 309 significantly different correlations, 299 were stronger in AGGs than NONs. The yellow module spanned olfactory cortical areas, the periventricular hypothalamus and brainstem regions. Of the 40 regions, 30 showed a significant difference in total connectivity, all of which were higher in the AGG module (Fig.4E). Of the 435 correlations examined, 177 were significantly different between AGGs and NONs, 173 of which showed higher correlations in AGGs (Fig. 4F).

The green network was a brainstem-heavy sensorimotor network with a few multimodal cortical regions. Of the 36 regions, 25 regions showed an increase in connectivity in the AGG module (Fig 5A-5B), with AGGs showing increased connectivity in 23 of the 25. When examining the individual correlations in the module 81 of 300 were significantly different between groups, 76 of which were higher in AGGs (Fig 5C). Although the connectivity profile was moderately preserved, we included the brown module in our analysis as it includes many of the regions which have been identified as the "social behavior network", such as the VMH, BNST, MEA, COAp, PMv, AHN and the MPOA. We found that AGGs has a significant increase in total connectivity in 35 of the 45 regions (Fig.5D-E). When examining the individual correlations, we found that 89 of the 630 correlations examined were significantly different, all of which were higher in AGGs.

When examining the female networks, we found that all AGG modules were moderately preserved in NONs based on the z-scored based metrics derived from permutation testing. Therefore, we chose to analyze the two modules with the weakest connectivity preservation based on the observed metrics. The turquoise module spanned somatosensory/interoceptive cortices, hippocampus, thalamus, and multiple regions in the midbrain. Of the 55 regions in the module 30

showed significant differences in total connectivity, 24 of which were increased in AGGs (Fig 6A-6B). Of the 465 correlations analyzed, 56 were significant with 47 showing higher correlations in AGGs. The brown module contained regions within sensory coritcal areas, amygdala and the lateral zone of the hypothalamus. Of the 44 total regions in this module AGGs showed an increase in connectivity in 20 of them (Fig. 6D-6E). Of the 190 correlations analyzed, 18 were significantly different all of which were higher in AGGs.

Discussion

This study reveals that aggressive social encounters reorganize brain-wide c-fos activation in a sex-dependent manner. Major sex differences were observed in the cortex and amygdala, with male AGGs showing significant increases in the somatosensory, interoceptive, and posterior polymodal cortices, while females showed preferential activation of anterior cortical regions. In addition, males demonstrated a broad increase across the entire amygdala complex. Females, in contrast only showed in increases in select regions of the basolateral complex. Midbrain activation patterns also differentiated the sexes. Males showed widespread activation across all layers of the superior colliculus, the dopaminergic ventral tegmental area and substansia nigra, and various midbrain regions related to motor output, whereas females showed concentrated increases in the deep layers of the colliculus, the PAG, DR and LC. In the hindbrain and cerebellum, males uniquely recruited reticulospinal/autonomic centers and cerebellar nodes, while females showed significant activation primarily in the inferior olive and a single vermal lobule. Together, these results suggest that aggression induces a reconfiguration of distributed mesoscale structures whose composition differ by sex.

Moving beyond regional counts, WGCNA provided a network perspective on this reorganization. We constructed separate networks for AGG and NON males and females, then formally tested whether AGG-defined modules were preserved in NON modules within each sex. Methodologically, WGCNA offered clear advantages over simple correlation maps. First, soft-thresholded, signed adjacency and topological overlap measure down-weight spurious connections and accentuate shared-neighborhood structure, yielding more stable modules than binarized or thresholded matrices (Zhang & Horvath, 2005). Second, permutation-based Z statistics disentangle density-level from connectivity-level preservation, highlighting modules that look intact in aggregate yet hide substantial rewiring of which region occupies central positions (Langfelder et al., 2011). Preservation analysis indicated that NON networks maintained the overall density of several AGG modules but failed to preserve the specific intra-module connectivity profiles in select cases suggesting that aggression reorganizes the connectivity profiles even when aggregate density is similar. Density-level preservation paired with connectivity-level changes suggest large-scale rewiring rather than simple up- or down-scaling of the same edges.

In males, the blue module exemplified large-scale strengthening with aggression. This community linked sensorimotor and interoceptive cortices with frontal areas, basal ganglia, septum, thalamic relays, and the superior colliculus. A large majority of its regions showed altered total connectivity, and most of those were stronger in AGG than NON, indicating module-wide gain increases. The yellow module (olfactory cortex, pallidal, preoptic/hypothalamic, and brainstem nodes) showed a similar pattern with three quarters of

regions increased total connectivity in AGG and most significant edges were stronger with aggression—again consistent with a high-gain state. The green, brainstem-heavy sensorimotor module also strengthened in AGG at both the region and edge levels. Surprisingly, the brown module which was composed of classic social-behavior regions (VMH, BNST, MEA, COAp, PMv, AHN, MPOA, AVPV) was moderately preserved at the module level. That there were increases in total connectivity, with relatively small differences in region specific correlations suggests that this module may simply scale-up activity in AGGs relative to NONs with changing functional connectivity patterns. This is in contrast to the other modules which showed broad changes in both total connectivity and the re-routing of paired correlations. Collectively, male aggression recruits a vertically integrated axis from cortex through basal ganglia, thalamus, superior colliculus, and brainstem, accompanied by enhanced coupling within olfactory hypothalamic assemblies

By contrast, female networks were more conservative. Preservation statistics indicated that AGG modules were generally maintained in NON, prompting focused analyses on the two least-preserved communities. The turquoise module (somatosensory/interoceptive cortex, hippocampus, lateral septum, thalamo-visual relays, multiple SC layers, and midbrain regions) showed selective increases in AGG—about half of the regions changed total connectivity and most significant edges were higher in AGG—while the brown module (olfactory, amygdala, hypothalamus, brainstem, thalamus) exhibited more modest remodeling with fewer significant edges overall, all favoring AGG. These results suggest that female aggression is supported by targeted potentiation within communities that bridge internal state (septum, hypothalamus), sensory integration (thalamo-visual relays, SC), and arousal hubs (midbrain), rather than by wholesale network-wide gain increases.

Several limitations warrant consideration. First, c-Fos is an indirect proxy of recent neuronal activation, lacks the temporal resolution to parse rapid dynamics or cell-type specific activation, and is unable to detect inhibition (Kovacs, 2008; Yang et al., 2024). Finally, while WGCNA emphasizes shared neighborhoods, module boundaries and colors are heuristic and depend on analytic choices (e.g., β, dynamic cut height), though we explicitly selected β to approximate scale-free topology.

These caveats point directly to future work. Causal tests in identified hubs could assess whether boosting or suppressing their activity shifts module structure and behavior in a sex-specific manner. The strong male bias toward a cortex→basal ganglia→thalamus/SC→brainstem axis suggests that perturbing nodes along this path may disproportionately alter escalation and motor release; the more selective female remodeling predicts greater sensitivity to manipulations of arousal-broadcast and evaluation hubs (e.g., intralaminar thalamus, LC/PAG). Pairing mesoscale c-Fos mapping with projection-defined or cell-type–specific calcium imaging would link community-level summaries to circuit motifs, while longitudinal designs could track whether module preservation and edge-level differences evolve across repeated encounters or hormonal states. Finally, integrating structural connectivity could help distinguish direct from polysynaptic co-activation.

In summary, aggression recruits distributed, mesoscale networks rather than isolated loci, and the architecture of this recruitment differs by sex. Males exhibit broad strengthening across a

vertically integrated sensorimotor-subcortical axis and olfactory/hypothalamic assemblies, whereas females show focused potentiation within communities bridging internal state, sensory integration, and arousal hubs. By leveraging WGCNA with module preservation and differential correlation, we uncover modules that are rewired in their internal connectivity, and we pinpoint the edges most sensitive to aggressive state. These insights provide a system-level framework for selecting candidate hubs and subnetworks for causal interrogation and, ultimately, for understanding how the brain orchestrates complex social behavior in a sex-specific manner.

Methods

Animals

Wild-type Swiss-Webster (SW) mice (male and female, 12-15 weeks; Charles River) were used as experimental (residents) mice. Intruders for the resident-intruder (RI) test were 8-12-week-old male or female C57/BL6J mice (Jackson Laboratory). All mice were allowed to acclimate to the housing facility for 1 week prior to any experimental protocol. Mice were paired with a member of the opposite sex for sexual experience for 9 weeks of age (females) for two weeks or at 11 weeks of age (males) for two days. Females were paired with castrated SW males (8-12 weeks; Charles River) to prevent pregnancy. All mice were maintained on a 12/12 h light/dark cycle (07:00–19:00) with *ad libitum* access to food and water. Housing and experimental rooms were maintained at 20–22 °C and 40–60% humidity. Experiments were conducted during the light phase. Procedures were performed in accordance with the National Institutes of Health Guide for Care and approved by the Use of Laboratory Animals and the Icahn School of Medicine at Mount Sinai Institutional Animal Care and Use Committee.

RI Test

Mice were screened using protocols adapted from previous studies(Aubry et al., 2022; Li et al., 2023). Cage tops were removed to monitor trials with an overhead camera (Sony HDR-CX440). A novel C57BL/6J mouse matching the sex of the resident was introduced into each cage and mice were allowed to freely interact for 5 min across three days. After 5 min elapsed, intruder mice were returned to their home cages. For female resident-intruder trials, cohabiting male mice were removed prior to the test and then returned to their home cages. Resident behaviors were manually annotated using Observer XT 11.5 (Noldus Interactive Technologies).

Perfusion, brain tissue processing, and imaging

For iDISCO+, mice were injected with 10% chloral hydrate and perfused transcardially with ice-cold 1× PBS (pH 7.4) following the third RI test. Tissue was fixed with cold 4% paraformaldehyde in 1× PBS. Brains were post-fixed for 12 h in the same fixative at 4 °C and then transferred to 1X PBS. The iDISCO+ staining protocol was modified from http://www.idisco.info. Fixed whole brains were incubated with the primary c-Fos antibody (no. 226003, 1:1,000, Synaptic Systems) and secondary donkey anti-rabbit IgG (H+L) Highly Cross-Adsorbed Secondary Antibody, Alexa Fluor 647 (no. A-31573, 1:1,000, Thermo Fisher Scientific) for 7 days each. A LaVision lightsheet microscope with zoom body was used for half-brain sagittal scanning, with dynamic focus and a step size of 4 µm.

Regional Count Analysis

Cleared brains were processed as previously described using ClearMap 1 (Renier et al., 2016; Renier et al., 2014). c-Fos^{+} cells were quantified using the cell detection module, with cell detection parameters optimized and validated based on the intensity and shape parameters of the signal. The autofluorescence channel was aligned to the Allen Institute's Common Coordinate Framework using the Elastix toolbox. We analyzed the resulting counts with a negative binomial generalized linear model in the MASS package using a log link including Sex**,** Pheno, and their interaction. For each fitted model, we obtained estimated marginal means and pairwise contrasts and controlled for FDR using the Benjamini and Hochberg procedure in prism. The negative binomial framework is appropriate for over dispersed counts because it models the mean–variance relationship directly. This workflow is preferable to two-way ANOVA on raw or transformed counts, which relies on Gaussian, homoscedastic residuals. Common fixes like log/square-root

transforms handle zeros poorly and often leave residual overdispersion, leading to inaccurate standard errors and p-values (O'Hara & Kotze, 2010) Moreover, tests built from models that better match the data distribution tend to have higher power than tests on transformed data (Wharton et al., 2016).

Network and module preservation analysis

To identify c-fos co-expression modules we performed Weighted Gene Co-expression Network Analysis (WGCNA) using the WGCNA R package (Langfelder and Horvath, 2008). A signed weighted adjacency matrix was constructed by computing pairwise Pearson correlations between all region pairs and raising the absolute value of each correlation to a soft-thresholding power β to approximate scale-free topology. The optimal β was selected using the pickSoftThreshold function to ensure that each network exhibited approximate scale-free topology ($R^2 > 0.8$). The adjacency matrix was transformed into a Topological Overlap Matrix (TOM), which measures the overlap in shared network neighbors between regions and reduces the influence of spurious or isolated connections. Regions were hierarchically clustered using average linkage on 1 – TOM dissimilarity, and modules were identified via dynamic tree cutting at a height of .25. Each module was assigned a unique color label and summarized by its module eigen-region, defined as the first principal component of the scaled expression matrix for regions within the module.

To assess differential connectivity of sex specific AGG and NON networks and their stability within datasets, we conducted module preservation analysis using the modulePreservation function. This analysis evaluates whether modules defined in a reference dataset (AGG) are preserved in a test dataset (NON), based on both network connectivity and density statistics. It also allows for the assessment of cluster quality based on the consistency of module structure across randomly partitioned subsets of the reference data. To assess the quality and preservation of modules, Z statistics were computed for each module. Each Z-score was calculated by comparing the observed module statistics to a null distribution generated from 500 permutation tests where module labels or sample labels were randomized. For a given statistic, the Z-score is calculated as: $Z = ((\text{observed} - \mu\_\text{null}) / \sigma\_\text{null})$ where μ_null and σ_null are the mean and standard deviation of the statistic under the null distribution. Larger Z-values indicate greater evidence of preservation or quality. The four z-statistics which comprises the density metric are:

meanSignAwareCor: measures the mean pair-wise signed Pearson correlations among every region pair inside the module in the test set. Strong preservation of this statistic indicates that the overall correlation (strength and direction) of the module remains tighter than assumed by the null distribution.

meanAdj: the average edge weight among module regions in the test network. A large Z for this statistic shows that the module still forms a densely connected block compared with modules generated by label permutations.

propVarExplained: quantifies how much of the within-module expression variance in the test data is still captured by the module eigen-region. A high, positive Z-score means the regions continue to behave collectively along a dominant expression axis.

meanSignAwareKME: evaluates the average signed module-membership (kME) values of all module genes in the test network. By retaining the sign information of each gene's correlation with the module eigengene, it asks whether genes remain positively or negatively aligned with that eigengene more strongly than in permuted data.

The z-statistics which comprise the connectivity measure are:
Zcor.KIM: evaluates the Pearson correlation between intramodular connectivity (kIM) vectors calculated in the reference and test networks. For each region, kIM is the sum of its edge weights to all other regions in the module. A high, positive Z-score indicates that the rank order of hubs versus peripheral genes is preserved far better than would be expected under random label permutations.

ZcorKME: captures the correlation between module-membership scores (kME) across the two datasets. kME is each region's correlation with the module eigen-region which reflects how strongly a regions's expression follows the module's dominant expression pattern. A high Z for this statistic means regions that were eigen-region aligned in the reference set remain similarly aligned in the test set, preserving the expression-centric notion of centrality.

Zcor.cor: measures the correlation between the entire matrices of pair-wise gene-gene correlations within the module in the reference and test data. Conceptually, all within-module correlations are flattened into a single vector for each dataset, and those two vectors are then correlated. A large Zcor.cor value signals that the strength of the correlations between regions in the module are preserved beyond chance.

We tested edge-level differences in functional coupling between aggressive and non-aggressive animals using Differential Correlation analysis with the DGCA framework (McKenzie et al., 2016). For each group, we assembled region × animal matrices of c-Fos activity and computed Pearson's correlation for every region pair. Correlations were z transformed, and edges were compared between groups using DGCA's two-sample z-test**.** Multiple testing was controlled with Benjamini–Hochberg FDR; significant edges ($q < 0.05$).

Ardinger, C. E., Chen, Y., Kimbrough, A., Grahame, N. J., & Lapish, C. C. (2024). Sex differences in neural networks recruited by frontloaded binge alcohol drinking. *Addict Biol*, *29*(9), e13434. https://doi.org/10.1111/adb.13434

Aubry, A. V., Durand-de Cuttoli, R., Karpman, E., Fisher-Foye, R. L., Parise, L. F., Cathomas, F., Burnett, C. J., Yang, Y., Yuan, C., LaBanca, A. R., Chan, K. L., Winston, K. T., Lin, H. Y., Dackour, F., Tavallaei, A. A., Alvarez, J., Nishioka, T., Morishita, H., Froemke, R. C.,…Russo, S. J. (2025). A crucial role for the cortical amygdala in shaping social encounters. *Nature*, *639*(8056), 1006-1015. https://doi.org/10.1038/s41586-024-08540-4

Aubry, A. V., Joseph Burnett, C., Goodwin, N. L., Li, L., Navarrete, J., Zhang, Y., Tsai, V., Durand-de Cuttoli, R., Golden, S. A., & Russo, S. J. (2022). Sex differences in appetitive and reactive aggression. *Neuropsychopharmacology*, *47*(10), 1746-1754. https://doi.org/10.1038/s41386-022-01375-5

Bayless, D. W., Yang, T., Mason, M. M., Susanto, A. A. T., Lobdell, A., & Shah, N. M. (2019). Limbic Neurons Shape Sex Recognition and Social Behavior in Sexually Naive Males. *Cell*, *176*(5), 1190-1205 e1120. https://doi.org/10.1016/j.cell.2018.12.041

Chen, A. X., Yan, J. J., Zhang, W., Wang, L., Yu, Z. X., Ding, X. J., Wang, D. Y., Zhang, M., Zhang, Y. L., Song, N., Jiao, Z. L., Xu, C., Zhu, S. J., & Xu, X. H. (2020). Specific Hypothalamic Neurons Required for Sensing Conspecific Male Cues Relevant to Inter-male Aggression. *Neuron*, *108*(4), 763-774 e766. https://doi.org/10.1016/j.neuron.2020.08.025

Falkner, A. L., Grosenick, L., Davidson, T. J., Deisseroth, K., & Lin, D. (2016). Hypothalamic control of male aggression-seeking behavior. *Nat Neurosci*, *19*(4), 596-604. https://doi.org/10.1038/nn.4264

Golden, S. A., Jin, M., Heins, C., Venniro, M., Michaelides, M., & Shaham, Y. (2019). Nucleus Accumbens Drd1-Expressing Neurons Control Aggression Self-Administration and Aggression Seeking in Mice. *J Neurosci*, *39*(13), 2482-2496. https://doi.org/10.1523/JNEUROSCI.2409-18.2019

Golden, S. A., Jin, M., & Shaham, Y. (2019). Animal Models of (or for) Aggression Reward, Addiction, and Relapse: Behavior and Circuits. *J Neurosci*, *39*(21), 3996-4008. https://doi.org/10.1523/JNEUROSCI.0151-19.2019

Goodson, J. L. (2005). The vertebrate social behavior network: evolutionary themes and variations. *Horm Behav*, *48*(1), 11-22. https://doi.org/10.1016/j.yhbeh.2005.02.003

Hashikawa, K., Hashikawa, Y., Tremblay, R., Zhang, J. X., Feng, J. E., Sabol, A., Piper, W. T., Lee, H., Rudy, B., & Lin, D. Y. (2017). Esr1(+) cells in the ventromedial hypothalamus control female aggression. *Nature Neuroscience*, *20*(11), 1580-+. https://doi.org/10.1038/nn.4644

Hong, W., Kim, D. W., & Anderson, D. J. (2014). Antagonistic control of social versus repetitive self-grooming behaviors by separable amygdala neuronal subsets. *Cell*, *158*(6), 1348-1361. https://doi.org/10.1016/j.cell.2014.07.049

Kessler, R. C., Coccaro, E. F., Fava, M., Jaeger, S., Jin, R., & Walters, E. (2006). The prevalence and correlates of DSM-IV intermittent explosive disorder in the National Comorbidity Survey Replication. *Arch Gen Psychiatry*, *63*(6), 669-678. https://doi.org/10.1001/archpsyc.63.6.669

Kimbrough, A., Lurie, D. J., Collazo, A., Kreifeldt, M., Sidhu, H., Macedo, G. C., D'Esposito, M., Contet, C., & George, O. (2020). Brain-wide functional architecture remodeling by

alcohol dependence and abstinence. *Proc Natl Acad Sci U S A*, *117*(4), 2149-2159. https://doi.org/10.1073/pnas.1909915117
Kovacs, K. J. (2008). Measurement of immediate-early gene activation- c-fos and beyond. *J Neuroendocrinol*, *20*(6), 665-672. https://doi.org/10.1111/j.1365-2826.2008.01734.x
Langfelder, P., & Horvath, S. (2008). WGCNA: an R package for weighted correlation network analysis. *BMC Bioinformatics*, *9*, 559. https://doi.org/10.1186/1471-2105-9-559
Langfelder, P., Luo, R., Oldham, M. C., & Horvath, S. (2011). Is my network module preserved and reproducible? *PLoS Comput Biol*, *7*(1), e1001057. https://doi.org/10.1371/journal.pcbi.1001057
Lawal, O. O., Lin, D., & Lischinsky, J. E. (2025). Estrogen Control of Social Behaviors. *Annu Rev Neurosci*, *48*(1), 125-147. https://doi.org/10.1146/annurev-neuro-112723-041639
Lee, H., Kim, D. W., Remedios, R., Anthony, T. E., Chang, A., Madisen, L., Zeng, H., & Anderson, D. J. (2014). Scalable control of mounting and attack by Esr1+ neurons in the ventromedial hypothalamus. *Nature*, *509*(7502), 627-632. https://doi.org/10.1038/nature13169
Li, L., Durand-de Cuttoli, R., Aubry, A. V., Burnett, C. J., Cathomas, F., Parise, L. F., Chan, K. L., Morel, C., Yuan, C., Shimo, Y., Lin, H. Y., Wang, J., & Russo, S. J. (2023). Social trauma engages lateral septum circuitry to occlude social reward. *Nature*, *613*(7945), 696-703. https://doi.org/10.1038/s41586-022-05484-5
Lin, D., Boyle, M. P., Dollar, P., Lee, H., Lein, E. S., Perona, P., & Anderson, D. J. (2011). Functional identification of an aggression locus in the mouse hypothalamus. *Nature*, *470*(7333), 221-226. https://doi.org/10.1038/nature09736
Lischinsky, J. E., & Lin, D. (2020). Neural mechanisms of aggression across species. *Nat Neurosci*, *23*(11), 1317-1328. https://doi.org/10.1038/s41593-020-00715-2
McCloskey, M. S., Kleabir, K., Berman, M. E., Chen, E. Y., & Coccaro, E. F. (2010). Unhealthy aggression: intermittent explosive disorder and adverse physical health outcomes. *Health Psychol*, *29*(3), 324-332. https://doi.org/10.1037/a0019072
McKenzie, A. T., Katsyv, I., Song, W. M., Wang, M., & Zhang, B. (2016). DGCA: A comprehensive R package for Differential Gene Correlation Analysis. *BMC Syst Biol*, *10*(1), 106. https://doi.org/10.1186/s12918-016-0349-1
Mei, L., Osakada, T., & Lin, D. (2023). Hypothalamic control of innate social behaviors. *Science*, *382*(6669), 399-404. https://doi.org/10.1126/science.adh8489
Mountoufaris, G., Nair, A., Yang, B., Kim, D. W., Vinograd, A., Kim, S., Linderman, S. W., & Anderson, D. J. (2024). A line attractor encoding a persistent internal state requires neuropeptide signaling. *Cell*, *187*(21), 5998-6015 e5918. https://doi.org/10.1016/j.cell.2024.08.015
Newman, E. L., Covington, H. E., III, Suh, J., Bicakci, M. B., Ressler, K. J., DeBold, J. F., & Miczek, K. A. (2019). Fighting females: Neural and behavioral consequences of social defeat stress in female mice [Peer Reviewed]. *Biological Psychiatry*, *.86*(9), pp. https://doi.org/10.1016/j.biopsych.2019.05.005 31255250
Newman, S. W. (1999). The medial extended amygdala in male reproductive behavior. A node in the mammalian social behavior network. *Ann N Y Acad Sci*, *877*, 242-257. https://doi.org/10.1111/j.1749-6632.1999.tb09271.x
Renier, N., Adams, E. L., Kirst, C., Wu, Z., Azevedo, R., Kohl, J., Autry, A. E., Kadiri, L., Umadevi Venkataraju, K., Zhou, Y., Wang, V. X., Tang, C. Y., Olsen, O., Dulac, C., Osten, P., & Tessier-Lavigne, M. (2016). Mapping of Brain Activity by Automated

Volume Analysis of Immediate Early Genes. *Cell*, *165*(7), 1789-1802. https://doi.org/10.1016/j.cell.2016.05.007

Renier, N., Wu, Z., Simon, D. J., Yang, J., Ariel, P., & Tessier-Lavigne, M. (2014). iDISCO: a simple, rapid method to immunolabel large tissue samples for volume imaging. *Cell*, *159*(4), 896-910. https://doi.org/10.1016/j.cell.2014.10.010

Roland, A. V., Coelho, C. A. O., Haun, H. L., Gianessi, C. A., Lopez, M. F., D'Ambrosio, S., Machinski, S. N., Kroenke, C. D., Frankland, P. W., Becker, H. C., & Kash, T. L. (2023). Alcohol Dependence Modifies Brain Networks Activated During Withdrawal and Reaccess: A c-Fos-Based Analysis in Mice. *Biol Psychiatry*, *94*(5), 393-404. https://doi.org/10.1016/j.biopsych.2023.01.018

Roy, D. S., Park, Y. G., Kim, M. E., Zhang, Y., Ogawa, S. K., DiNapoli, N., Gu, X., Cho, J. H., Choi, H., Kamentsky, L., Martin, J., Mosto, O., Aida, T., Chung, K., & Tonegawa, S. (2022). Brain-wide mapping reveals that engrams for a single memory are distributed across multiple brain regions. *Nature Communications*, *13*(1), 1799. https://doi.org/10.1038/s41467-022-29384-4

Simpson, S., Chen, Y., Wellmeyer, E., Smith, L. C., Aragon Montes, B., George, O., & Kimbrough, A. (2021). The Hidden Brain: Uncovering Previously Overlooked Brain Regions by Employing Novel Preclinical Unbiased Network Approaches. *Front Syst Neurosci*, *15*, 595507. https://doi.org/10.3389/fnsys.2021.595507

Stagkourakis, S., Spigolon, G., Williams, P., Protzmann, J., Fisone, G., & Broberger, C. (2018). A neural network for intermale aggression to establish social hierarchy. *Nat Neurosci*, *21*(6), 834-842. https://doi.org/10.1038/s41593-018-0153-x

Unger, E. K., Burke, K. J., Jr., Yang, C. F., Bender, K. J., Fuller, P. M., & Shah, N. M. (2015). Medial amygdalar aromatase neurons regulate aggression in both sexes. *Cell Rep*, *10*(4), 453-462. https://doi.org/10.1016/j.celrep.2014.12.040

Vetere, G., Kenney, J. W., Tran, L. M., Xia, F., Steadman, P. E., Parkinson, J., Josselyn, S. A., & Frankland, P. W. (2017). Chemogenetic Interrogation of a Brain-wide Fear Memory Network in Mice. *Neuron*, *94*(2), 363-374 e364. https://doi.org/10.1016/j.neuron.2017.03.037

Wei, D., Talwar, V., & Lin, D. (2021). Neural circuits of social behaviors: Innate yet flexible. *Neuron*, *109*(10), 1600-1620. https://doi.org/10.1016/j.neuron.2021.02.012

Yamaguchi, T., Wei, D., Song, S. C., Lim, B., Tritsch, N. X., & Lin, D. (2020). Posterior amygdala regulates sexual and aggressive behaviors in male mice. *Nat Neurosci*, *23*(9), 1111-1124. https://doi.org/10.1038/s41593-020-0675-x

Yan, R., Wei, D., Varshneya, A., Shan, L., Dai, B., Asencio, H. J., 3rd, Gollamudi, A., & Lin, D. (2024). The multi-stage plasticity in the aggression circuit underlying the winner effect. *Cell*, *187*(24), 6785-6803 e6718. https://doi.org/10.1016/j.cell.2024.09.030

Yang, B., Karigo, T., & Anderson, D. J. (2022). Transformations of neural representations in a social behaviour network. *Nature*, *608*(7924), 741-749. https://doi.org/10.1038/s41586-022-05057-6

Yang, D., Wang, Y., Qi, T., Zhang, X., Shen, L., Ma, J., Pang, Z., Lal, N. K., McClatchy, D. B., Seradj, S. H., Leung, V. H., Wang, K., Xie, Y., Polli, F. S., Maximov, A., Gonzalez, O. C., de Lecea, L., Cline, H. T., Augustine, V.,…Ye, L. (2024). Phosphorylation of pyruvate dehydrogenase inversely associates with neuronal activity. *Neuron*, *112*(6), 959-971 e958. https://doi.org/10.1016/j.neuron.2023.12.015

Zha, X., Wang, L., Jiao, Z. L., Yang, R. R., Xu, C., & Xu, X. H. (2020). VMHvl-Projecting Vglut1+ Neurons in the Posterior Amygdala Gate Territorial Aggression. *Cell Rep*, *31*(3), 107517. https://doi.org/10.1016/j.celrep.2020.03.081

Zhang, B., & Horvath, S. (2005). A general framework for weighted gene co-expression network analysis. *Stat Appl Genet Mol Biol*, *4*, Article17. https://doi.org/10.2202/1544-6115.1128

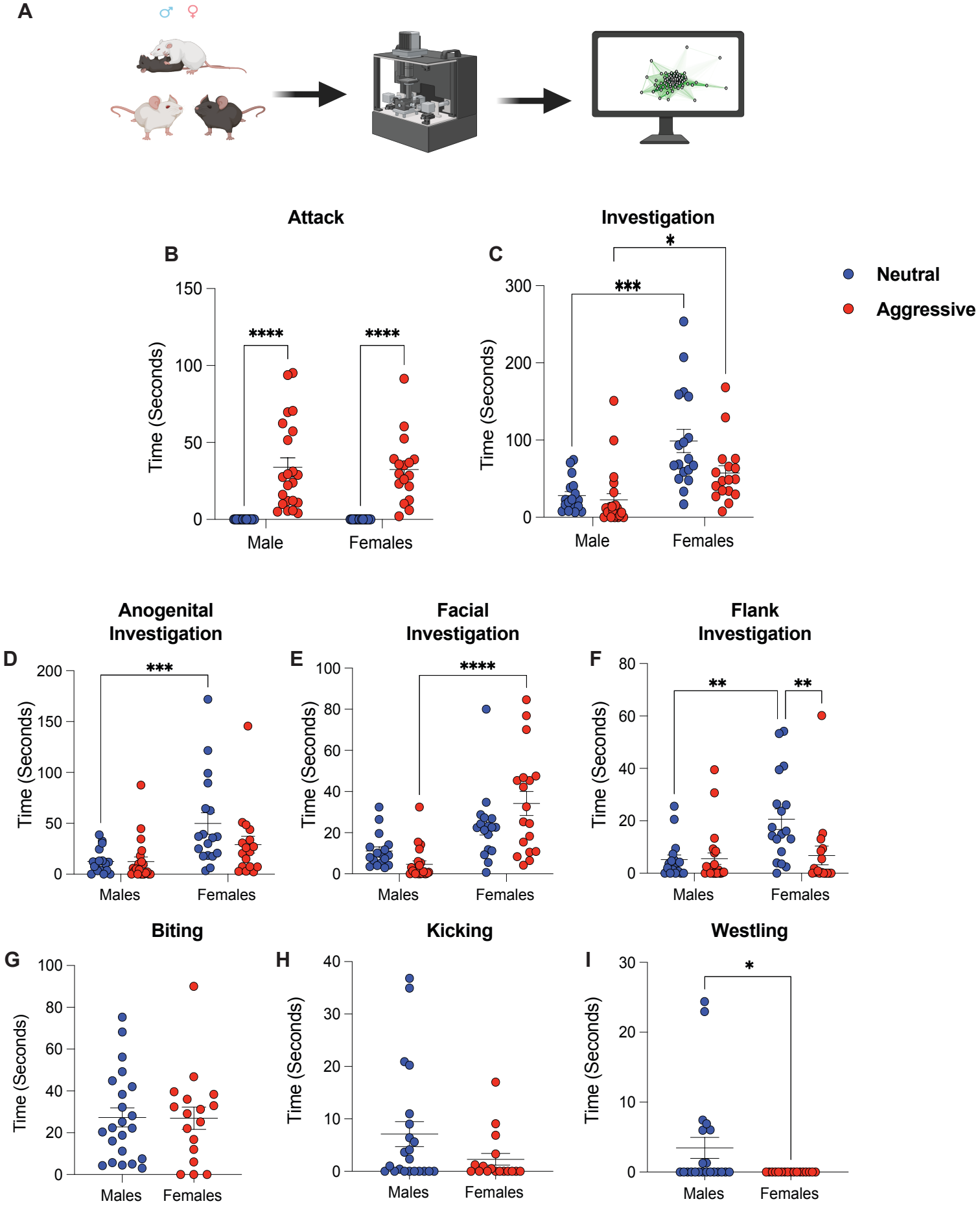
A
B
Attack
Time (Seconds)
150
100
50
0
****
****
Male
Females
C
Investigation
300
200
100
0
*
***
Male
Females
Neutral
Aggressive
D
Anogenital Investigation
200
150
100
50
0
***
Males
Females
E
Facial Investigation
100
80
60
40
20
0
****
Males
Females
F
Flank Investigation
80
60
40
20
0
**
**
Males
Females
G
Biting
100
80
60
40
20
0
Males
Females
H
Kicking
40
30
20
10
0
Males
Females
I
Westling
30
20
10
0
*
Males
Females

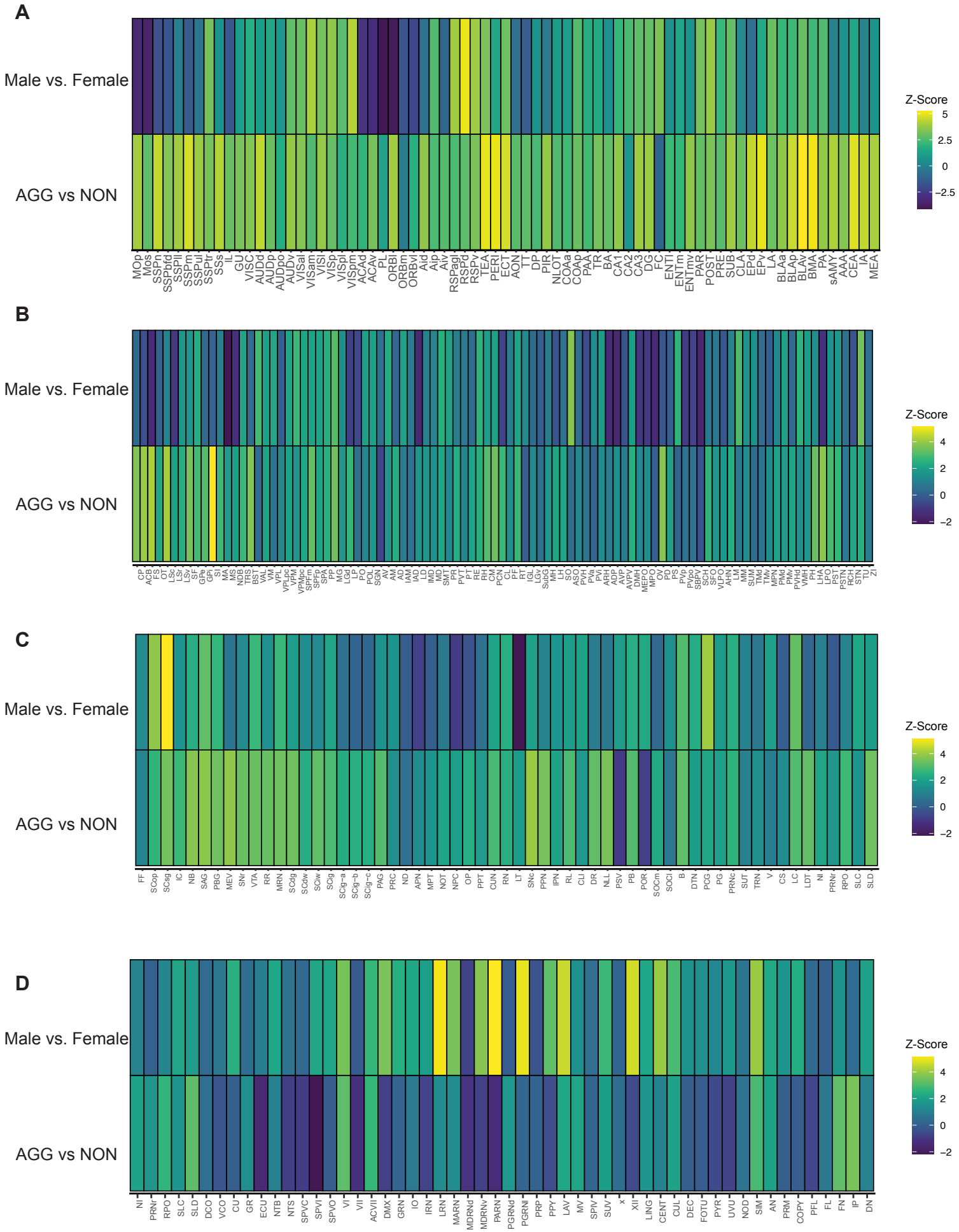
A
Male vs. Female
AGG vs NON
Z-Score
5
2.5
0
−2.5
MOp MOs SSPn SSPbfd SSPll SSPm SSPul SSPtr SSs IL GU VISC AUDd AUDp AUDpo AUDv VISal VISam VISl VISp VISpl VISpm ACAd ACAv PL ORBl ORBm ORBvl AId AIp AIv RSPagl RSPd RSPv TEA PERI ECT AON TT DP PIR NLOT COAa COAp PAA TR BA CA1 CA2 CA3 DG FC ENTl ENTm ENTmv PAR POST PRE SUB CLA EPd EPv LA BLAa BLAp BLAv BMA PA sAMY AAA CEA IA MEA
B
Male vs. Female
AGG vs NON
Z-Score
4
2
0
−2
CP ACB FS OT LSc LSr LSv SF GPe GPi SI MA MS NDB TRS BST VAL VM VPL VPLpc VPM VPMpc SPFm SPFp SPA PP MG LGd LP PO POL SGN AV AM AD IAM IAD LD IMD MD SMT PR PVT PT RE RH CM PCN CL PF RT IGL LGv SubG MH LH SO ASO PVH PVa PVi ARH ADP AVP AVPV DMH MEPO MPO OV PD PS PVp PVpo SBPV SCH SFO VLPO AHN LM MM SUM TMd TMv MPN PMd PMv PVHd VMH PH LHA LPO PST PSTN RCH STN TU ZI
C
Male vs. Female
AGG vs NON
Z-Score
4
2
0
−2
FF SCop SCsg IC NB SAG PBG MEV SNr VTA RR MRN SCdg SCdw SCiw SCig SCig−a SCig−b SCig−c PAG PRC ND APN MPT NOT NPC OP PPT CUN RN LT SNc PPN IPN RL CLI DR NLL PSV PB POR SOCm SOCl B DTN PCG PG PRNc SUT TRN V CS LC LDT NI PRNr RPO SLC SLD
D
Male vs. Female
AGG vs NON
Z-Score
4
2
0
−2
NI PRNr RPO SLC SLD DCO VCO CU GR ECU NTB NTS SPVC SPVI SPVO VI VII ACVII DMX GRN IO IRN LRN MARN MDRNd MDRNv PARN PGRNd PGRNl PRP PPY LAV MV SPIV SUV x XII LING CENT CUL DEC FOTU PYR UVU NOD SIM AN PRM COPY PFL FL FN IP DN

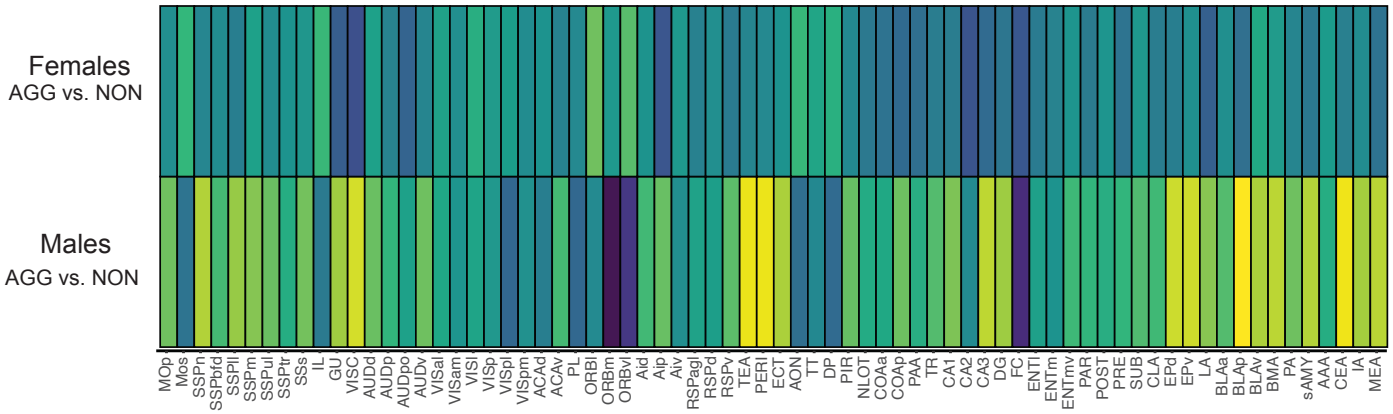
Females
AGG vs. NON
Males
AGG vs. NON
Z
4
2
0
−2
MOp
Mos
SSPn
SSPbfd
SSPll
SSPm
SSPul
SSPtr
SSs
IL
GU
VISC
AUDd
AUDp
AUDpo
AUDv
VISal
VISam
VISl
VISp
VISpl
VISpm
ACAd
ACAv
PL
ORBl
ORBm
ORBvl
Aid
Aip
Aiv
RSPagl
RSPd
RSPv
TEA
PERI
ECT
AON
TT
DP
PIR
NLOT
COAa
COAp
PAA
TR
CA1
CA2
CA3
DG
FC
ENTl
ENTm
ENTmv
PAR
POST
PRE
SUB
CLA
EPd
EPv
LA
BLAa
BLAp
BLAv
BMA
PA
sAMY
AAA
CEA
IA
MEA

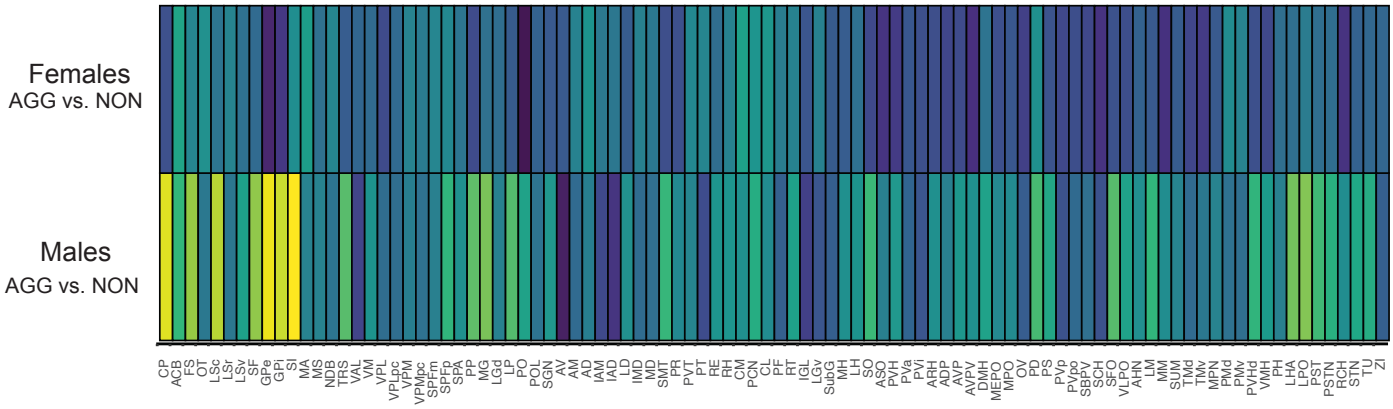
Females
AGG vs. NON
Males
AGG vs. NON
Z
4
2
0
CP
ACB
FS
OT
LSc
LSr
LSv
GPe
GPi
SI
MA
MS
NDB
TRS
VAL
VM
VPL
VPLpc
VPM
VPMpc
SPFm
SPFp
SPA
PP
MG
LGd
LP
PO
POL
SGN
AV
AM
AD
IAM
IAD
LD
IMD
MD
SMT
PR
PVT
PT
RE
RH
CM
PCN
CL
PF
RT
IGL
LGv
SubG
MH
LH
SO
ASO
PVH
PVa
PVi
ARH
ADP
AVP
AVPV
DMH
MEPO
MPO
OV
PD
PS
PVp
PVpo
SBPV
SCH
SFO
VLPO
ALIM
LIM
MM
SUM
TMd
TMv
MPN
PMd
PMv
PVHd
VMH
FH
LHA
LPA
PST
PSTN
RCH
STN
TU
ZI

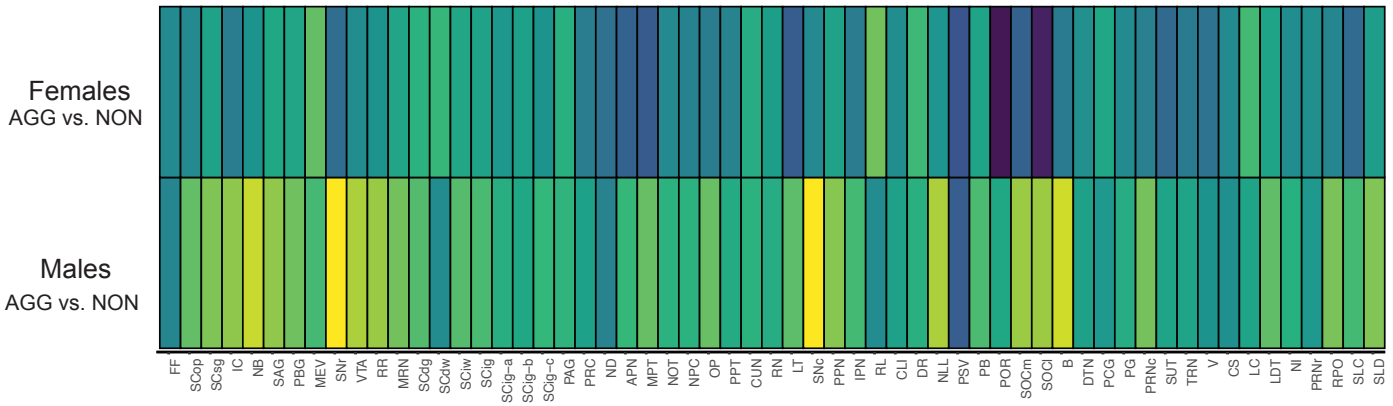
Females
AGG vs. NON
Males
AGG vs. NON
Z
2.5
0.0
−2.5
FF
SCop
SCsg
IC
NB
SAG
PBG
MEV
SNr
VTA
RR
MRN
SCdg
SCdw
SCiw
SCig
SCig−a
SCig−b
SCig−c
PAG
PRC
ND
APN
MPT
NOT
NPC
OP
PPT
CUN
RN
LT
SNc
PPN
IPN
RL
CLi
DR
NLL
PSV
PB
POR
SOCm
SOCl
B
DTN
PCG
PG
PRNc
SUT
TRN
V
CS
LC
LDT
NI
PRNr
RPO
SLC
SLD

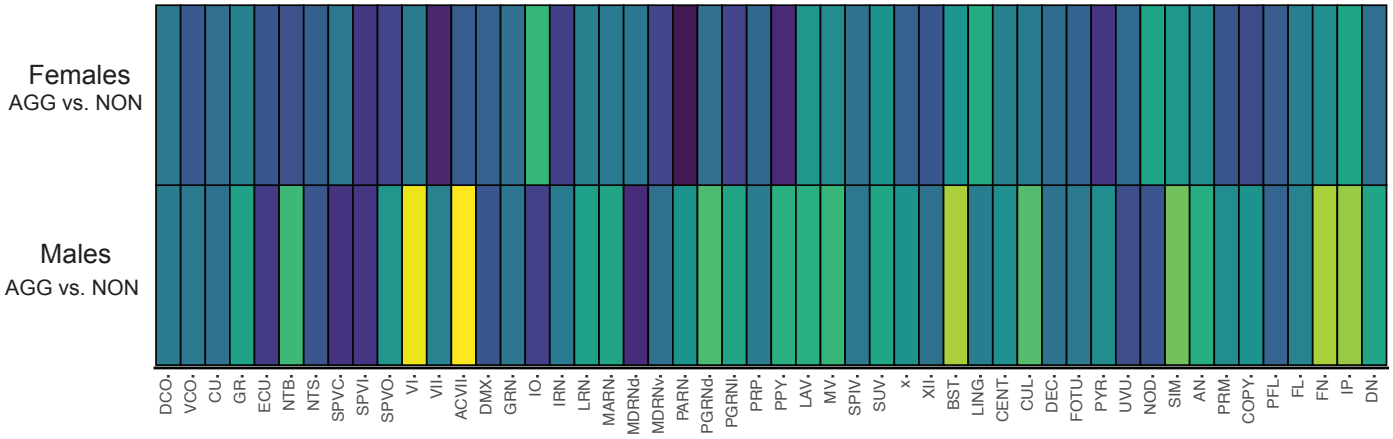
Females
AGG vs. NON
Males
AGG vs. NON
Z
5.0
2.5
0.0
−2.5
DCO.
VCO.
CU.
GR.
ECU.
NTB.
NTS.
SPVC.
SPVI.
SPVO.
VI.
VII.
ACVII.
DMX.
GRN.
IO.
IRN.
LRN.
MARN.
MDRNd.
MDRNv.
PARN.
PGRNd.
PGRNl.
PRP.
PPY.
LAV.
MV.
SPIV.
SUV.
x.
XII.
BST.
LING.
CENT.
CUL.
DEC.
FOTU.
PYR.
UVU.
NOD.
SIM.
AN.
PRM.
COPY.
PFL.
FL.
FN.
IP.
DN.

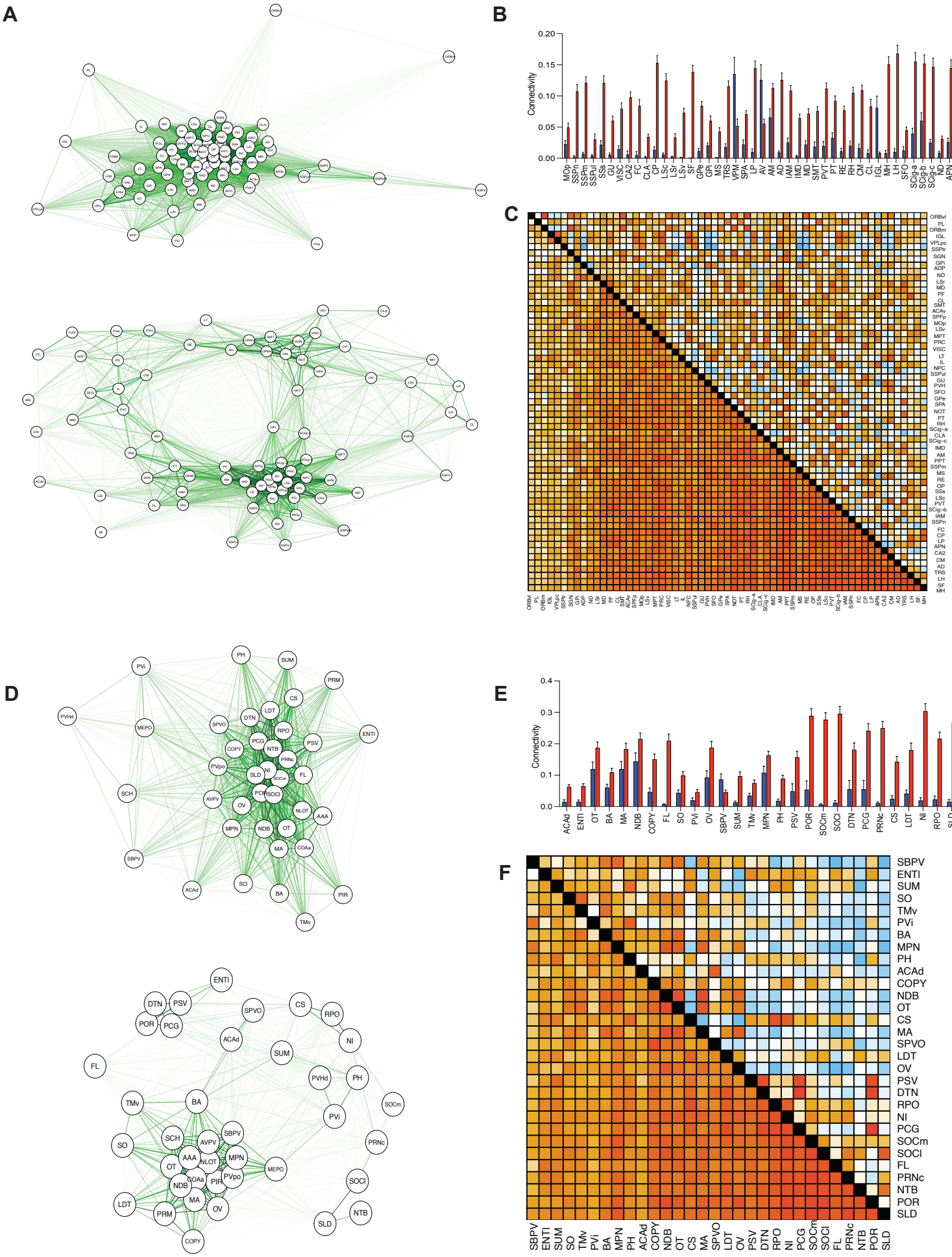
A
B
Connectivity
0.20
0.15
0.10
0.05
0.00
MOp SSPn SSPm SSPul SSs GU VISC CA2 FC CLA CP LSc LSr LSv SF GPe GPi MS TRS VPM SPA LP AV AM AD IAM IMD MD SMT PVT PT RE RH CM CL IGL MH LH SFO SCig-a SCig-b SCig-c ND APN MPT NOT OP PPT LT
C
D
PVi PH SUM PRM PVHd MEPO SPVO DTN LDT CS ENTl RPO PCG NTB PSV COPY PRNc PVpo SLD NI FL SOCm SCH AVPV POR SOCl OV NLOT AAA MPN NDB OT MA COAa SBPV ACAd SO BA PIR TMv
E
Connectivity
0.4
0.3
0.2
0.1
0.0
ACAd ENTl OT BA MA NDB COPY FL SO PVi OV SBPV SUM TMv MPN PH PSV POR SOCm SOCl DTN PCG PRNc CS LDT NI RPO SLD NTB SPVO
F
SBPV ENTl SUM SO TMv PVi BA MPN PH ACAd COPY NDB OT CS MA SPVO LDT OV PSV DTN RPO NI PCG SOCm SOCl FL PRNc NTB POR SLD

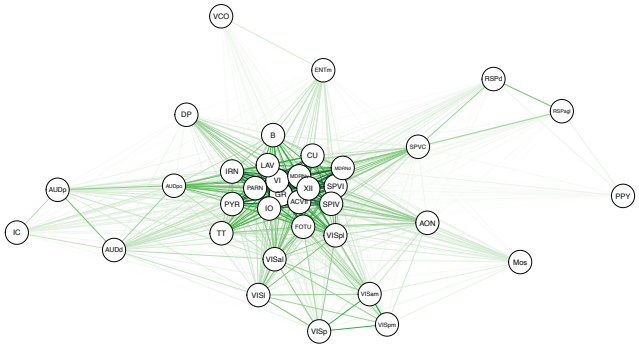
VCO
ENTm
RSPd
RSPagl
DP
B
CU
SPVC
IRN
LAV
MDRNv
VI
XII
SPVI
AUDp
AUDpo
PARN
GR
PYR
IO
ACVII
SPIV
PPY
IC
TT
FOTU
AON
AUDd
VISpl
VISal
Mos
VISl
VISam
VISp
VISpm

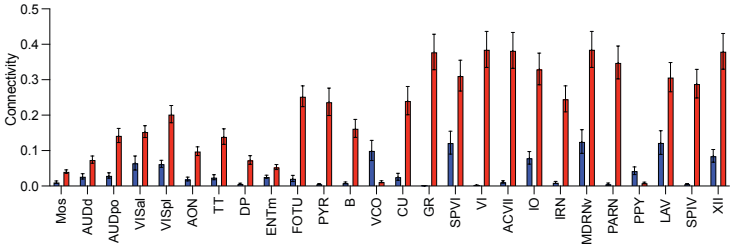
Connectivity
0.5
0.4
0.3
0.2
0.1
0.0
Mos
AUDd
AUDpo
VISal
VISpl
AON
TT
DP
ENTm
FOTU
PYR
B
VCO
CU
GR
SPVI
VI
ACVII
IO
IRN
MDRNv
PARN
PPY
LAV
SPIV
XII

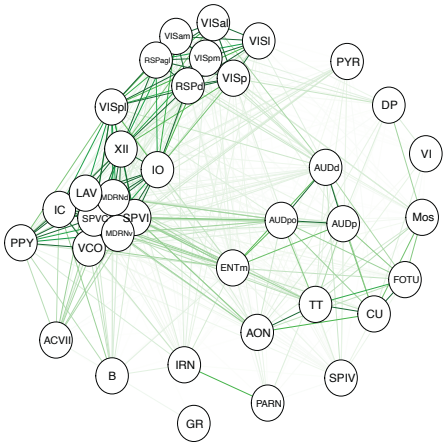
VISal
VISam
VISl
RSPagl
VISpm
VISp
RSPd
PYR
VISpl
DP
XII
IO
VI
AUDd
LAV
MDRNd
IC
SPVC
SPVI
AUDpo
AUDp
Mos
PPY
MDRNv
VCO
ENTm
FOTU
TT
CU
AON
ACVII
IRN
B
SPIV
PARN
GR

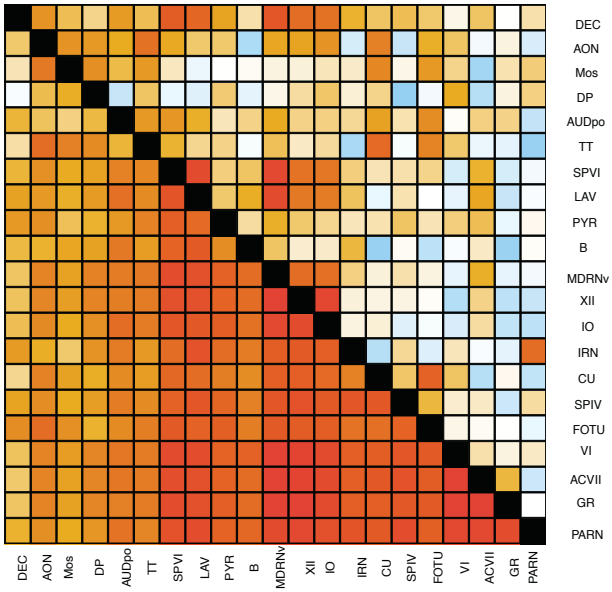
DEC
AON
Mos
DP
AUDpo
TT
SPVI
LAV
PYR
B
MDRNv
XII
IO
IRN
CU
SPIV
FOTU
VI
ACVII
GR
PARN

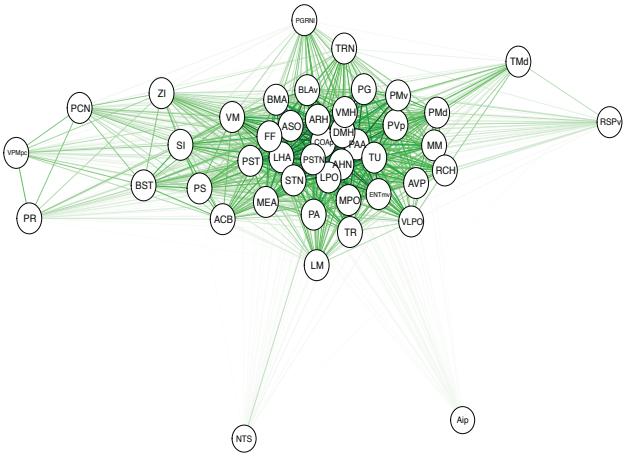
PGRNl
TRN
TMd
ZI
BLAv
PG
PMv
PCN
BMA
VMH
PMd
VM
ASO
ARH
PVp
RSPv
FF
DMH
SI
COAp
PAA
MM
VPMpc
PST
LHA
PSTN
AHN
TU
RCH
BST
PS
STN
LPO
AVP
ENTmv
MEA
MPO
PR
ACB
PA
VLPO
TR
LM
NTS
Aip

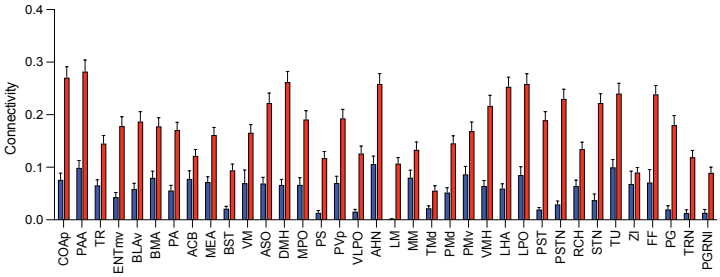
Connectivity
0.4
0.3
0.2
0.1
0.0
COAp
PAA
TR
ENTmv
BLAv
BMA
PA
ACB
MEA
BST
VM
ASO
DMH
MPO
PS
PVp
VLPO
AHN
LM
MM
TMd
PMd
PMv
VMH
LHA
LPO
PST
PSTN
RCH
STN
TU
ZI
FF
PG
TRN
PGRNl

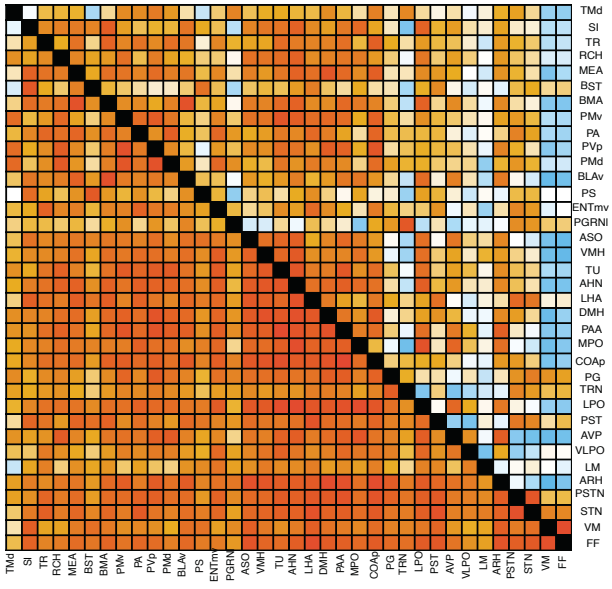
TMd
SI
TR
RCH
MEA
BST
BMA
PMv
PA
PVp
PMd
BLAv
PS
ENTmv
PGRNl
ASO
VMH
TU
AHN
LHA
DMH
PAA
MPO
COAp
PG
TRN
LPO
PST
AVP
VLPO
LM
ARH
PSTN
STN
VM
FF

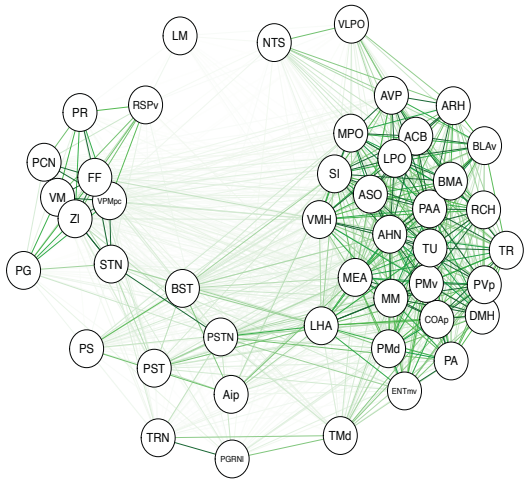
LM
NTS
VLPO
AVP
ARH
PR
RSPv
MPO
ACB
BLAv
PCN
FF
LPO
SI
BMA
VM
VPMpc
ASO
PAA
RCH
ZI
VMH
AHN
TU
TR
PG
STN
MEA
PMv
PVp
BST
MM
COAp
DMH
LHA
PS
PSTN
PMd
PA
PST
Aip
ENTmv
TRN
TMd
PGRNl

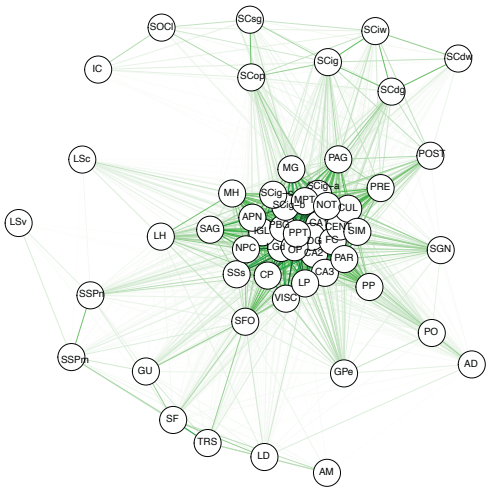
SOCl
SCsg
SCiw
SCdw
IC
SCig
SCop
SCdg
LSc
POST
PAG
MG
PRE
MH
SCig-a
MPT
NOT
CUL
LSv
APN
PBG
CA1
CENT
SIM
LH
SAG
IGL
PPT
DG
FC
NPC
LGd
OP
CA2
PAR
SGN
SSs
CP
CA3
LP
PP
SSPn
VISC
SFO
PO
SSPm
GU
GPe
AD
SF
TRS
LD
AM

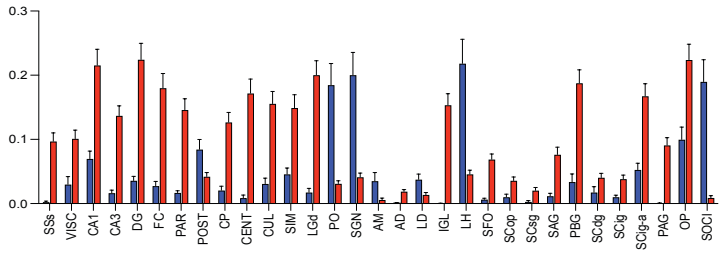
0.3
0.2
0.1
0.0
SSs
VISC
CA1
CA3
DG
FC
PAR
POST
CP
CENT
CUL
SIM
LGd
PO
SGN
AM
AD
LD
IGL
LH
SFO
SCop
SCsg
SAG
PBG
SCdg
SCig
SCig-a
PAG
OP
SOCl

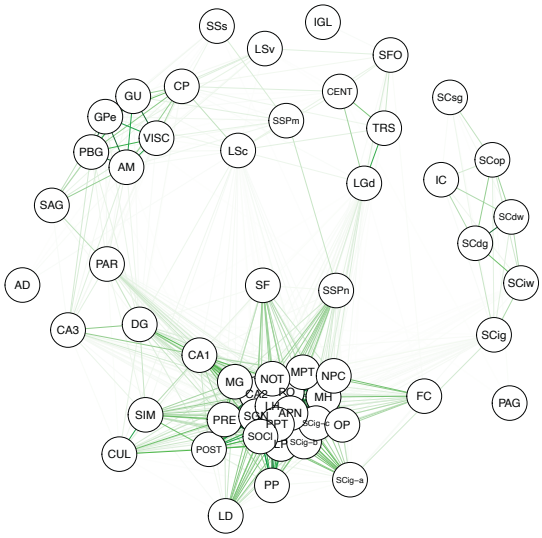
SSs
IGL
LSv
SFO
CP
CENT
SCsg
GU
GPe
SSPm
TRS
VISC
PBG
LSc
SCop
AM
LGd
IC
SAG
SCdw
SCdg
PAR
SCiw
AD
SF
SSPn
CA3
DG
SCig
CA1
MG
NOT
MPT
NPC
FC
PAG
SIM
PRE
SGN
ARN
MH
OP
CUL
POST
SOCl
PP
SCig-a
LD

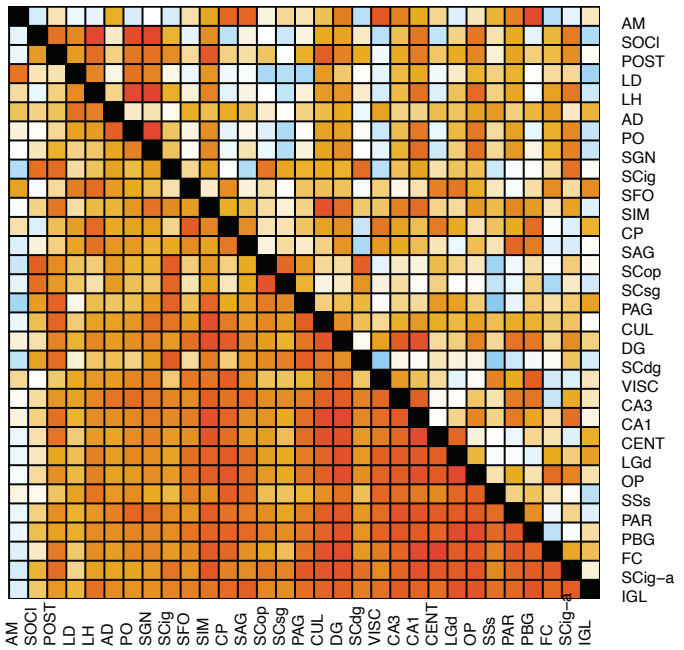
AM
SOCl
POST
LD
LH
AD
PO
SGN
SCig
SFO
SIM
CP
SAG
SCop
SCsg
PAG
CUL
DG
SCdg
VISC
CA3
CA1
CENT
LGd
OP
SSs
PAR
PBG
FC
SCig−a
IGL

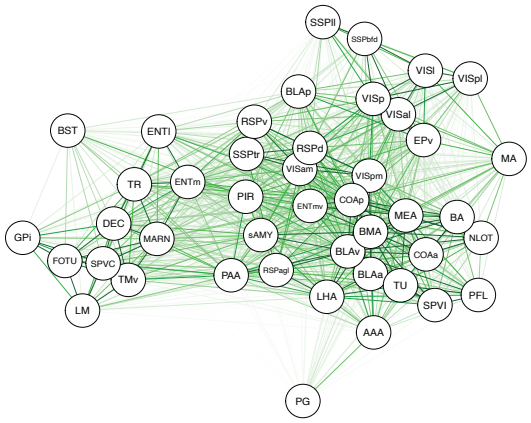
SSPll
SSPbfd
VISl
VISpl
BLAp
VISp
VISal
BST
ENTl
RSPv
EPv
SSPtr
RSPd
MA
VISam
VISpm
TR
ENTm
PIR
COAp
ENTmv
MEA
BA
DEC
GPi
MARN
sAMY
BMA
NLOT
FOTU
SPVC
BLAv
COAa
TMv
PAA
RSPagl
BLAa
TU
LHA
PFL
LM
SPVI
AAA
PG

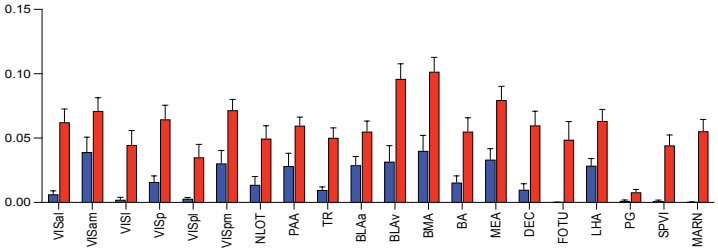
0.15
0.10
0.05
0.00
VISal
VISam
VISl
VISp
VISpl
VISpm
NLOT
PAA
TR
BLAa
BLAv
BMA
BA
MEA
DEC
FOTU
LHA
PG
SPVI
MARN

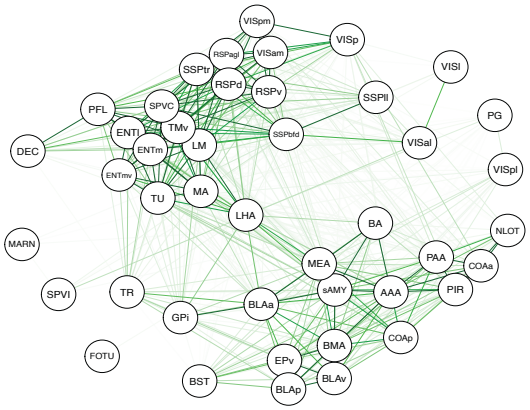
VISpm
VISp
RSPagl
VISam
SSPtr
VISl
RSPd
RSPv
SSPll
PFL
SPVC
PG
ENTl
TMv
SSPbfd
DEC
ENTm
LM
VISal
ENTmv
VISpl
TU
MA
LHA
BA
NLOT
MARN
MEA
PAA
COAa
SPVI
TR
sAMY
AAA
PIR
BLAa
GPi
COAp
BMA
FOTU
EPv
BST
BLAv
BLAp

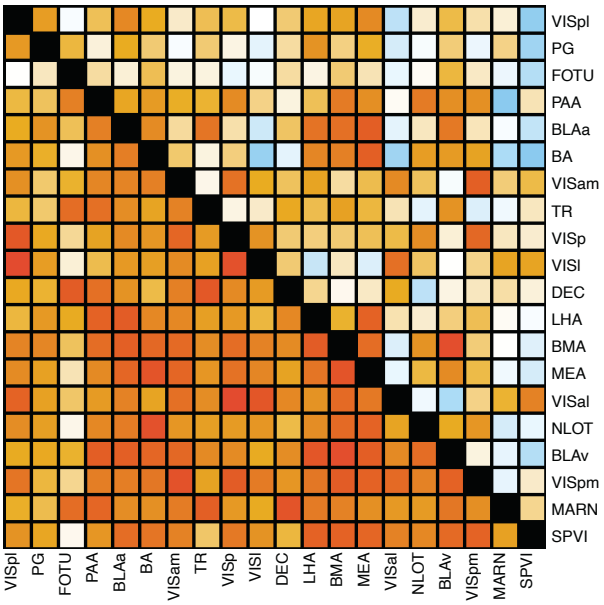
VISpl
PG
FOTU
PAA
BLAa
BA
VISam
TR
VISp
VISl
DEC
LHA
BMA
MEA
VISal
NLOT
BLAv
VISpm
MARN
SPVI